Spin conversion and pick-off annihilation of ortho-positronium in gaseous xenon at elevated temperatures

Kengo Shibuya,[1,*] Takashi Nakayama,[1] Haruo Saito,[1] and Toshio Hyodo[2]
[1]*Institute of Physics, Graduate School of Arts and Sciences, The University of Tokyo, Komaba 3-8-1, Meguro, Tokyo 153-8902, Japan*
[2]*Institute of Materials Structure Science, High Energy Accelerator Organization, Oho 1-1, Tsukuba, Ibaraki 305-0801, Japan*
(Received 17 April 2013; published 15 July 2013)

We present experimental results for the annihilation rate of ortho-positronium in gaseous xenon at 250 kPa using a digital-oscilloscope-based positron annihilation lifetime spectrometer as a function of temperature (300–623 K). Owing to the Zeeman mixing of positronium in a magnetic field, the annihilation rate is divided into two components: one is due to ortho-para postronium spin conversion induced by spin-orbit interaction, while the other is due to pick-off annihilation. The spin-conversion annihilation rate is proportional to $T^{2.1}$, where T is the temperature. We attributed this dependence to the fact that the spin conversion occurs only in p-wave scattering during positronium–xenon collisions and to the fact that, after thermalization of the ortho-positronium atoms, their velocity profile follows a Maxwell-Boltzmann distribution. The results also show that the pick-off annihilation rate is almost linear in temperature. This increase is a dependence exceptionally stronger than that observed in other gases.

DOI: 10.1103/PhysRevA.88.012511 PACS number(s): 36.10.Dr, 78.70.Bj, 34.80.Uv

I. INTRODUCTION

Positronium (Ps) is a hydrogenlike bound state of an electron and a positron. This metastable atom consists of matter and antimatter and decays into γ-ray photons. Three γ-ray photons are produced from the Ps triplet spin state $|S = 1, M = -1, 0, 1\rangle$ and two γ-ray photons are produced from the singlet spin state $|S = 0, M = 0\rangle$ (S is the total spin quantum number and M is the z component). Triplet Ps is called ortho-positronium (o-Ps), and singlet Ps is called para-positronium (p-Ps). In vacuum their annihilation rates (i.e., inverse lifetimes) are $\lambda_o = 7.0401(7) \times 10^6$ s^{-1} {$\tau_o =$ 142.04(1) ns [1–4]} and $\lambda_p = 7.9909(17) \times 10^9$ s^{-1} {$\tau_p =$ 125.14(3) ps [4–6]}, respectively. Because of the conservation laws of momentum, energy, angular momentum, and charge parity, the annihilation photons possess rich information about preannihilation experiences of Ps as well as Ps states at the time of annihilation.

The lifetime of o-Ps is so long after formation that many collisions with gas molecules precede the annihilation. These collisions open four Ps annihilation pathways in which two γ-ray photons are emitted [7,8]: (i) ortho-para spin conversion due to the spin-orbit interaction, (ii) pick-off annihilation, (iii) ortho-para spin conversion due to electron exchange, and (iv) chemical quenching. The first path was theoretically proposed by Mitroy and Novikov in 2003 [9] to explain why Ps formation fraction in gaseous Xe is much less than that in gaseous He ("Xe problem" [10]). This reaction was experimentally confirmed in 2006 [11]. The first path is opened by a high-Z atom in the gas molecule. Once o-Ps converts into p-Ps, it quickly annihilates because $\lambda_p \gg \lambda_o$. The second path is open for any gas molecule. A positron in an o-Ps atom can annihilate with an electron in an atomic or molecular orbital. The third path is open for paramagnetic gas molecules with unpaired electrons such as O_2 and NO [12–15]. The last path is open when a Ps atom chemically binds or enters a resonance state with a gas molecule such as NO_2, Br_2, or I_2 [16,17].

In this study we measured the o-Ps annihilation rates Λ_1 and Λ_2 for the first and second path, respectively, in gaseous Xe ($Z = 54$) at 250.0(4) kPa and in the temperature range of 300–623 K. Theoretically [9], the first path (i.e., ortho-para spin conversion due to spin-orbit interaction) is forbidden in s-wave scattering and allowed in p-wave and higher-order scattering. Previously we reported that Λ_1 is greater than Λ_2 for Ps–Xe collisions [11], which indicates that p-wave scattering is considerable in Ps–Xe collisions even at room temperature (RT). Given that $\sigma_p \propto E^2$, the temperature dependence of Λ_1 is approximated to be $\Lambda_1 \propto \sigma_p v \propto E^2 v \propto v^5 \propto T^{2.5}$, where σ_p is the p-wave scattering cross section, E is Ps kinetic energy, and T is temperature. Thus, we expect a remarkably strong temperature dependence of Λ_1 at elevated temperatures, which differs considerably from weak temperature dependences observed in many gases where the first path is closed both below [18–23] and above RT [24–26]. According to Mitroy and Novikov [9], such a strong temperature dependence is necessary for their theory to provide the final answer for the Xe problem. Although Heyland [27] reported a large increase in the annihilation rate in Xe–H_2 mixed gas from 273 to 373 K, they did not observe this increase in pure Xe gas and offered no explanation for these results.

We emphasize that Λ_1 is attributed to p-wave scattering and it can be separately determined from the other paths. This direct correspondence allows a clear comparison of experimental and theoretical results. Another advantage of this system is that a small change in the temperature results in a large change in the two-photon annihilation rate. This is because, as shown in this paper, the p-wave cross section has a strong energy dependence. We can study the properties of Ps–Xe collisions by controlling the Ps kinetic energy without using a UV laser [28] nor an accelerator [29].

*shibuken@gakushikai.jp

 ©2013 American Physical Society

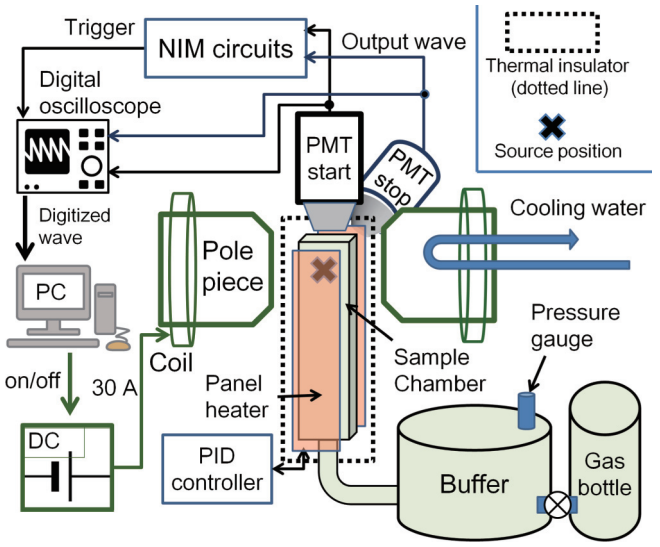

FIG. 1. (Color online) Schematic of experimental setup. The NIM circuits consisted of delay lines, discriminators (model 935, ORTEC), gate stretchers (KN1500, Kaizu, Japan), and a coincidence unit (RPN130, REPIC, Japan). The position of the source and the silica aerogel is indicated by a bold X.

II. EXPERIMENT

A. Experimental setup

The experimental setup was essentially the same as that previously used [11,30] and is summarized below.

The positron source was 50 kBq (1.3 μCi) of ^{22}NaCl deposited on KAPTON films. The source was sandwiched by 0.1 g cm^{-3} silica aerogel (SAG) [31,32]. SAG was used as a positron–positronium converter; approximately half of the injected positrons formed Ps in the free volume between the ultrafine silica grains.

As shown in Fig. 1, the source and SAG were positioned inside a stainless-steel sample chamber near the top (sample-chamber dimensions were 30 mm × 15 mm × 200 mm). Panel heaters covered the two largest faces of the sample chamber, and the chamber and heaters were wrapped with aluminum foil and thermal insulator. The temperature of the two points on the chamber faces nearest to the source were monitored with two type-E thermocouples and maintained at 300, 423, 540, 588, and 623 K with an uncertainty less than 1 K using a PID feedback controller. The bottom of the sample chamber was connected to a larger gas buffer where the pressure was continuously monitored and maintained at 250 kPa for all measurements. A bottle of research grade Xe gas was connected to the buffer. The chamber was positioned at the center of the pole pieces of a conventional electromagnet that applied a magnetic field of $B = 0.83(2)$ T at the position of the positron source. For each set of experimental parameters, the data acquisition lasted about 10 days. Measurements without Xe gas were also done to estimate the effects of SAG.

Our positron annihilation lifetime (PAL) spectrometer is based on a digital oscilloscope [33–35]. Two scintillation detectors were used: one for the start signals, and the other for the stop signals. The start signal was due to a 1.27 MeV nuclear γ ray, which is immediately emitted after positron emission, and the stop signal was due to annihilation radiation with energy at or below 511 keV, which is emitted during pair annihilation. Each detector employed a BaF_2 crystal optically coupled with a photomultiplier tube (H6614Q-70MOD, Hamamatsu, Japan) for high-magnetic-field environments. The anode outputs were transferred to both a digital oscilloscope (WaveRunner 6050, LeCroy) and NIM circuits. Detecting coincidence between the start and stop signals, the NIM circuits sent a trigger signal to the oscilloscope. Upon receiving the trigger signal, the oscilloscope recorded the digitized waveforms and sent them to a PC.

At the PC, the time interval between the start and stop signals were analyzed using a constant fraction method. In this analysis, irregular waveforms with a nonflat base line, an abnormal rise time, and multiple peaks were rejected [33]. The time-interval histogram constituted the PAL spectrum. The spectra exhibited a prompt peak that was attributed to singlet Ps as well as free positrons followed by a long-lived tail that was attributed to triplet Ps. After subtracting the background noise, we fitted the tail to a single exponential function. Typical fitting time range was 170–400 ns after the prompt peak. This time range allowed Ps atoms to be sufficiently thermalized so that the annihilation rate was essentially constant within the statistical uncertainty.

B. Data analysis

In a magnetic field two Ps states $|1,\pm1\rangle$ are not affected, whereas the other two Ps states are mixed by the Zeeman effect; the new states are $|+\rangle = (1/\sqrt{1+y^2})|1,0\rangle - (y/\sqrt{1+y^2})|0,0\rangle$ and $|-\rangle = (y/\sqrt{1+y^2})|1,0\rangle + (1/\sqrt{1+y^2})|0,0\rangle$, where $y = x/(\sqrt{1+x^2}+1)$ with $x = 4\mu_0 B/\Delta E$; μ_0 is the magnetic moment of the electron (positron) and ΔE is the Ps hyperfine splitting. Ps in the $|\pm\rangle$ states can decay into two or three γ-ray photons. Under a magnetic field of B, in vacuum, the annihilation rate (i.e., inverse lifetime) of $|+\rangle$ is $\lambda_+ = 1.08 \times 10^8$ s^{-1} ($\tau_+ = 9.27$ ns $\ll \tau_o$) and that of $|-\rangle$ is $\lambda_- = 7.87 \times 10^9$ s^{-1} ($\tau_- = 127$ ps $\approx \tau_p$). When spin conversion occurs during Ps–Xe collisions, the lifetime of $|1,\pm1\rangle$ is affected by a magnetic field because, since $\lambda_+ \gg \lambda_o$, Ps in the $|+\rangle$ state quickly annihilates once converted from $|1,\pm1\rangle$ before the inverse reaction occurs [11,30].

The annihilation rate is obtained by the following rate equations describing Ps populations, N_i, with $i = 1, 2, 3, 4$ corresponding to the four states $|+\rangle$, $|-\rangle$, $|1,1\rangle$, and $|1,-1\rangle$, respectively:

$$\frac{d}{dt}\begin{pmatrix} N_1(t) \\ N_2(t) \\ N_3(t) \\ N_4(t) \end{pmatrix} = A \begin{pmatrix} N_1(t) \\ N_2(t) \\ N_3(t) \\ N_4(t) \end{pmatrix}, \quad (1)$$

$$A\,(k_{\rm SC},\lambda_{\rm PO}) = \begin{pmatrix} -\lambda_+ - k_{\rm SC}(\xi+2) - \lambda_{\rm PO} & k_{\rm SC}\xi & k_{\rm SC}\eta & k_{\rm SC}\zeta \\ k_{\rm SC}\xi & -\lambda_- - k_{\rm SC}(\xi+2) - \lambda_{\rm PO} & k_{\rm SC}\zeta & k_{\rm SC}\eta \\ k_{\rm SC}\eta & k_{\rm SC}\zeta & -\lambda_o - 2k_{\rm SC} - \lambda_{\rm PO} & 0 \\ k_{\rm SC}\zeta & k_{\rm SC}\eta & 0 & -\lambda_o - 2k_{\rm SC} - \lambda_{\rm PO} \end{pmatrix}. \quad (2)$$

The off-diagonal elements of A represent the conversion probabilities, where $k_{\rm SC}$ is the reaction rate and ξ, η, and ζ are parameters that depend on the magnetic field as follows [6,22]: $\xi = (1-y^2)^2/(1+y^2)^2$, $\eta = (1-y)^2/(1+y^2)$, and $\zeta = (1+y)^2/(1+y^2)$. The diagonal elements possess additional terms: the pick-off annihilation rate $\lambda_{\rm PO}$ for any Ps state, the self-annihilation rates $\lambda_+ = \frac{1}{1+y^2}\lambda_o + \frac{y^2}{1+y^2}\lambda_p$ for $|+\rangle$, $\lambda_- = \frac{y^2}{1+y^2}\lambda_o + \frac{1}{1+y^2}\lambda_p \approx \lambda_p$ for $|-\rangle$, and λ_o for $|1,\pm1\rangle$.

As SAG is used in the measurements, we should consider the effects. $k_{\rm SC}$ and $\lambda_{\rm PO}$ are divided into two factors:

$$k_{\rm SC} = k_{\rm SC}^{\rm Xe} + k_{\rm SC}^{\rm SAG} \equiv k_{\rm SC}^{\rm Xe+SAG}, \quad (3)$$

$$\lambda_{\rm PO} = \lambda_{\rm PO}^{\rm Xe} + \lambda_{\rm PO}^{\rm SAG} \equiv \lambda_{\rm PO}^{\rm Xe+SAG}, \quad (4)$$

where $k_{\rm SC}^{\rm Xe}$ is the spin-conversion rate due to Xe, $k_{\rm SC}^{\rm SAG}$ is that due to SAG, $\lambda_{\rm PO}^{\rm Xe}$ is the pick-off annihilation rate due to Xe, and $\lambda_{\rm PO}^{\rm SAG}$ is that due to SGA.

The lifetime of the long-lived components is the inverse of the least eigenvalue of $A(\lambda_{\rm PO},k_{\rm SC})$. On the one hand, we have four independent variables in Eqs. (2)–(4), $k_{\rm SC}^{\rm Xe+SAG}$, $k_{\rm SC}^{\rm SAG}$, $\lambda_{\rm PO}^{\rm Xe+SAG}$, and $\lambda_{\rm PO}^{\rm SAG}$, while on the other hand, we measure four lifetimes of the long-lived components under four different conditions: at zero magnetic field or nonzero magnetic field of B with Xe gas or without Xe gas (see Table I). Then, the four independent variables are determined by a least-squares analysis.

III. RESULTS

The measured lifetimes are summarized in Table I. As the results of the least-squares analysis, $k_{\rm SC}^{\rm SAG}$ is determined to be zero within the uncertainty at all temperatures [e.g., $k_{\rm SC}^{\rm SAG} = (0 \pm 4) \times 10^3\ {\rm s}^{-1}$ at RT]; we consider the second path as the only path possible in SAG. Therefore, $\Lambda_1 \equiv k_{\rm SC}^{\rm Xe} = k_{\rm SC}^{\rm Xe+SAG} - k_{\rm SC}^{\rm SAG} = k_{\rm SC}^{\rm Xe+SAG}$, while $\Lambda_2 \equiv \lambda_{\rm PO}^{\rm Xe} = \lambda_{\rm PO}^{\rm Xe+SAG} - \lambda_{\rm PO}^{\rm SAG}$.

Λ_1 and Λ_2 are normalized to ${}_1Z_{\rm eff}^{\rm SC} = \Lambda_1/4\pi r_0^2 nc$ and ${}_1Z_{\rm eff}^{\rm PO} = \Lambda_2/4\pi r_0^2 nc$, respectively, where r_0 is the classical electron radius, n is the number density of gas molecules, and c is the velocity of light. These values are also listed in Table I. The normalized annihilation rates obtained at 300 K are consistent with those previously reported: ${}_1Z_{\rm eff}^{\rm SC} = 0.77(12)$ and ${}_1Z_{\rm eff}^{\rm PO} = 0.48(12)$ [11].

The normalized annihilation rates are plotted against temperature in Fig. 2 and the curves are fit to power laws in T to model the temperature dependence. The solid lines in Fig. 2 are the results of the least-square fit described as follows:

$${}_1Z_{\rm eff}^{\rm SC} = 4.56(10) \times 10^{-6} \times T^{2.08(1)} \quad (5)$$

and

$${}_1Z_{\rm eff}^{\rm PO} = 1.65(7) \times 10^{-3} \times T^{1.03(1)}. \quad (6)$$

In addition, the pick-off annihilation rate due to SAG, which is free from Xe gas, is

$$\lambda_{\rm PO}^{\rm SAG}(T) = 9.91(7) \times 10^4 \times T^{0.317(1)}. \quad (7)$$

IV. DISCUSSION

A. Spin conversion due to spin-orbit interaction during Ps–Xe collisions

As described in Eq. (5), the annihilation rate Λ_1 is proportional to $T^{2.08(1)}$ during Ps–Xe collisions. This temperature dependence is less than the approximation $\Lambda_1 \propto \sigma_p(v)v \propto T^{2.5}$.

For improving the approximation, we first consider a proposed formula for σ_p described as

$$\sigma_p(k) = \frac{12\pi \sin^2\delta_p}{k^2}, \qquad k^3 \cot\delta_p \approx -\frac{1}{a} + \frac{r}{2}k^2, \quad (8)$$

where k is the Ps wave number, δ_p is the phase shift, a is the scattering length, and r is the effective range [9,36]. The unit of length is the Bohr radius. Because (a, r) are not available for xenon, we use those of hydrogen ($a = 6.8, r = -4.1$ [9,36]) to obtain $\sigma_p \propto E^{1.73}$ for $E \leqslant 100$ meV. Thus, Λ_1

TABLE I. Ps lifetimes and annihilation rates.

	Ps lifetime in SAG (ns)		Ps lifetime in Xe and SAG (ns)			
Temperature (K)	0.83 T	0.00 T	0.83 T	0.00 T	${}_1Z_{\rm eff}^{\rm SC}$	${}_1Z_{\rm eff}^{\rm PO}$
300	131.5 ± 0.3	131.5 ± 0.2	89.7 ± 0.5	100.7 ± 0.3	0.69 ± 0.04	0.60 ± 0.05
423	128.8 ± 0.3	129.0 ± 0.2	82.9 ± 0.4	95.7 ± 0.3	1.30 ± 0.05	0.80 ± 0.07
540	127.2 ± 0.3	127.5 ± 0.3	75.2 ± 0.4	89.9 ± 0.3	2.26 ± 0.10	1.00 ± 0.12
588	128.9 ± 0.3	129.5 ± 0.2	73.2 ± 0.5	88.3 ± 0.4	2.67 ± 0.14	1.23 ± 0.17
623	128.7 ± 0.3	128.7 ± 0.2	70.4 ± 0.5	85.8 ± 0.3	3.11 ± 0.14	1.36 ± 0.17

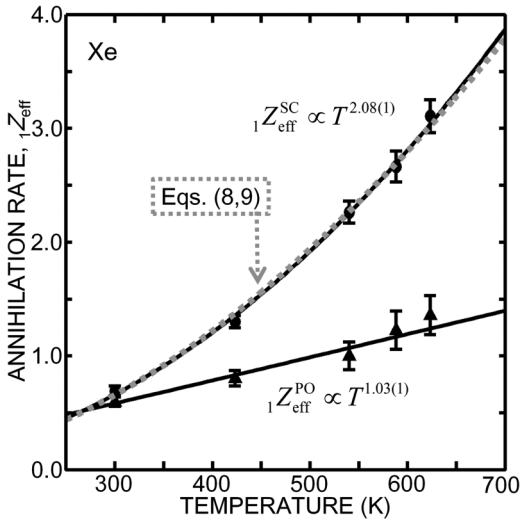

FIG. 2. Annihilation rates plotted as a function of temperature. The spin-conversion annihilation rate $_1Z_{\rm eff}^{\rm SC}$ is plotted with circles, and the pick-off annihilation rate $_1Z_{\rm eff}^{\rm PO}$ is plotted with triangles. The black solid lines are the results from fit for each data set, as described in Eqs. (5) and (6). The gray dotted line shows the result of a calculation using the p-wave scattering cross section and the Maxwell-Boltzmann distribution, as described in Eqs. (8) and (9).

depends on temperature as $\Lambda_1 \propto \sigma_p(v)v \propto T^{2.23}$, which is still inconsistent with the experimental result of $\Lambda_1 \propto T^{2.08(1)}$.

Second, we consider a Maxwell-Boltzmann distribution of the Ps atoms. With a Ps velocity distribution $[\rho(v)]$ the averaged Λ_1 over Ps velocity (v) is described as

$$\bar{\Lambda}_1 = n f_{\rm SC} \int \rho(v)\,\sigma_p(v) v\,dv \Big/ \int \rho(v)\,dv, \qquad (9)$$

where $f_{\rm SC}$ is the spin-conversion probability per p-wave scattering event. Here a Maxwell-Boltzmann distribution can be used for $\rho(v)$ because Ps atoms are considered to be thermalized over the typical time range of the PAL analysis: 170–400 ns from the prompt peak.

By using Eqs. (8) and (9) simultaneously, we obtain a good agreement between the measurement points and calculated curve (gray dotted line) as shown in Fig. 2. The sole adjustable parameter in the fitting is $f_{\rm SC}$, which is found to be $f_{\rm SC} = 8.8 \times 10^{-4}$. Thus, although we use (a, r) of hydrogen instead of xenon, the result explains the power-law dependence $\lambda \propto T^{2.08(1)}$. Mitroy and Novikov [9] underestimated Λ_1 and presented a slightly smaller value: $f_{\rm SC} = 5.3 \times 10^{-4}$.

We must consider the Ps velocity distribution when calculating $\bar{\Lambda}_1$. To explain the importance of this, in Fig. 3 we show the Maxwell-Boltzmann distribution for Ps $[F(v)]$ at 623 K, the Ps–H p-wave scattering cross section, and the result for $\Lambda_1(v)$ obtained as the products $F(v)\sigma_p(v)v$. The annihilation rate $\Lambda_1(v)$ peaks at $v = 168.3$ km/s, which is considerably faster than the most probable velocity of 97.2 km/s and the root-mean-square velocity of 119.0 km/s. This fact indicates that most annihilation via the first path occurs at the high-energy tail of $F(v)$ because of the strong energy dependence of Λ_1.

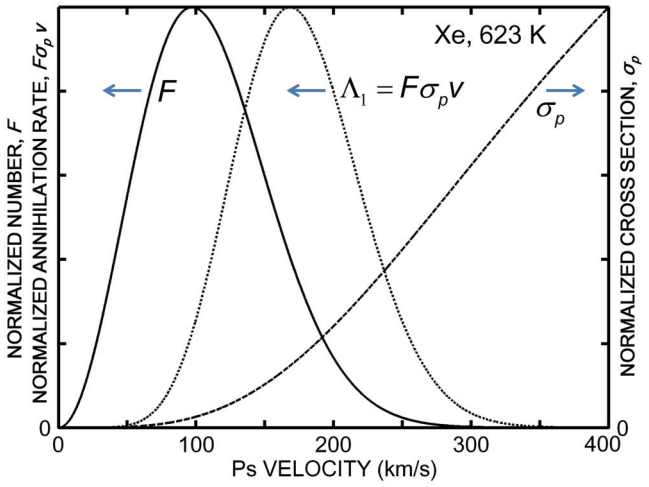

FIG. 3. (Color online) Maxwell-Boltzmann distribution of Ps at 623 K (solid line, normalized) peaking at 97.2 km/s, Ps–H p-wave scattering cross section (dashed line, normalized) increasing monotonically, and Ps spin-conversion annihilation rate (dotted line, normalized) peaking at 168.3 km/s. Most annihilations occur in the high-energy tail of the Maxwell-Boltzmann distribution because of the strong energy dependence.

This selective annihilation does not change $F(v)$ because the momentum transfer cross section is estimated to be much larger than $f_{\rm SC}\sigma_p$.

Next, we discuss the difference in ortho-para spin conversion via the first and third paths considering the temperature dependences of the annihilation rates. According to Kiefl [15], the annihilation rate during Ps–O_2 collisions, without the first path, increased by approximately 40% with the increase in temperature from 295 to 632 K. This increased annihilation rate is attributed mainly to the third path because the annihilation rate Λ_3 is approximately 60 times larger than Λ_2 at RT [13]. The temperature dependence of Λ_3 during

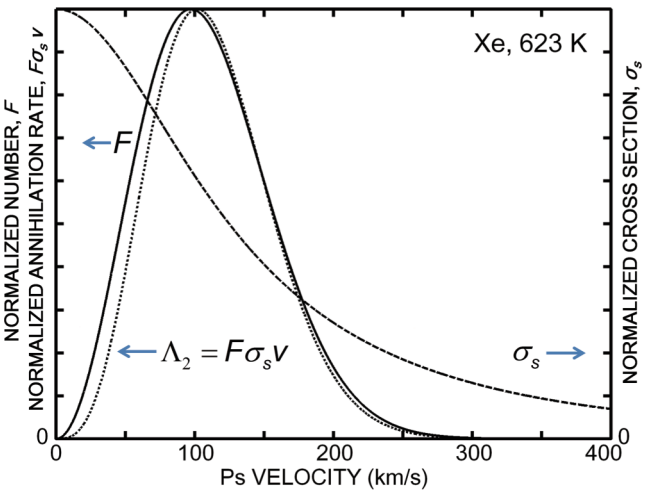

FIG. 4. (Color online) Maxwell-Boltzmann distribution of Ps at 623 K (solid line, normalized) peaking at 97.2 km/s, Ps–H s-wave scattering cross section (dashed line, normalized) decreasing monotonically, and Ps pick-off annihilation rate (dotted line, normalized) peaking at 101.7 km/s.

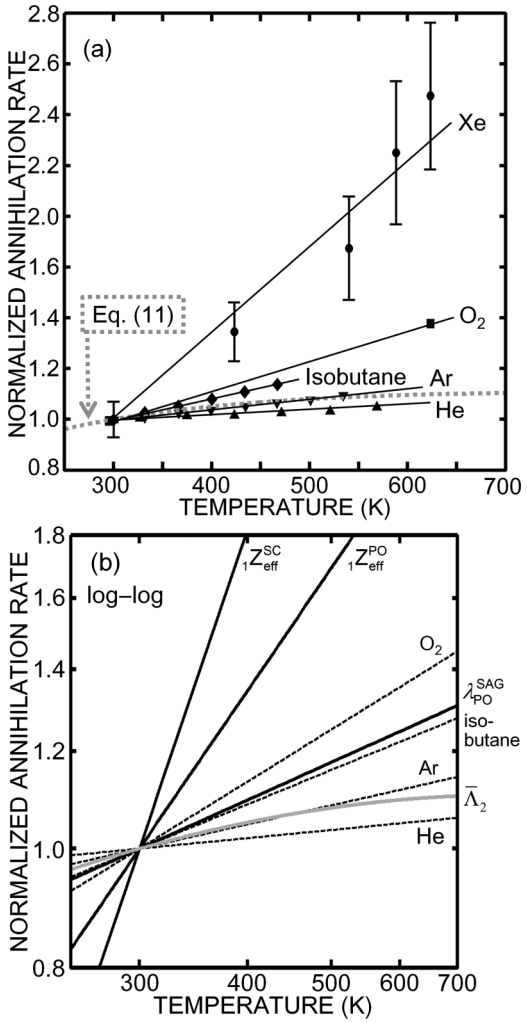

FIG. 5. (a) Pick-off annihilation rates for He (triangles [24]), Ar (nablas [24]), isobutane (diamonds [24]), O_2 (squares [15]), and Xe (circles, this study). The gray dotted line is the result of Eq. (11). The vertical axis is normalized to unity at 300 K. Lines are to guide the eye. (b) Log–log plots of annihilation rates normalized to unity at 300 K. Solid lines are the results of Eqs. (5), (6), and (7). The gray solid line is the result of Eq. (11). Dashed lines are for O_2 [15], isobutane [24], Ar [24], and He [24].

Ps–O_2 collisions is much weaker than that of Λ_1 during Ps–Xe collisions. The latter increased by 350 ± 30% with an increase in temperature from 300 to 623 K. This large difference in the temperature dependencies is not surprising because both Ps ortho-para spin conversions, the first and third paths, arise from completely different mechanisms. We attribute the difference partly to the order of the dominant partial wave for spin conversion: s-wave scattering for Λ_3 and p-wave scattering for Λ_1.

B. Pick-off annihilation during Ps–Xe collisions

As described in Eq. (6), the annihilation rate Λ_2 during Ps–Xe collisions is proportional to $T^{1.03(1)}$. As a first approximation, Λ_2 is assumed to be proportional to the s-wave scattering cross section σ_s. A proposed formula for σ_s is

$$\sigma_s(k) = \frac{4\pi \sin^2 \delta_s}{k^2}, \qquad k \cot \delta_s \approx -\frac{1}{a} + \frac{r}{2}k^2, \tag{10}$$

where δ_s is the phase shift [9,36]. The averaged Λ_2 is described as

$$\bar{\Lambda}_2 = n f_{\mathrm{PO}} \int \rho(v)\, \sigma_s(v) v\, dv \Big/ \int \rho(v)\, dv, \tag{11}$$

where f_{PO} is the pick-off annihilation probability per s-wave scattering event. $\sigma_s(v)$ monotonically decreases, as shown in Fig. 4.

The results of Eq. (11) indicate that $\bar{\Lambda}_2$ increased by 9.8% with an increase in temperature from 300 to 623 K, as shown in Fig. 5(a) (gray dotted line). This result is similar to those for Λ_2 of many gases above RT, as reported by Vallery *et al.* [24]. For comparison, we plot the results for He, Ar, and isobutane in Figs. 5(a) and 5(b). However, the annihilation rate Λ_2 during Ps–Xe collisions increases by 130 ± 30% with an increase in temperature from 300 to 623 K. The origin of such a strong temperature dependence of Λ_2 during Ps–Xe collisions is not yet understood.

Figure 5(b) shows the annihilation rates as a function of temperature on a log–log scale. The vertical axis is normalized to unity at 300 K. The values ${}_1Z^{\mathrm{SC}}_{\mathrm{eff}}$ and ${}_1Z^{\mathrm{PO}}_{\mathrm{eff}}$ are given by Eqs. (5) and (6), respectively, and $\lambda^{\mathrm{SAG}}_{\mathrm{PO}}$ is given by Eq. (7). The average annihilation rate $\bar{\Lambda}_2$ is calculated using Eq. (11). The annihilation rates for O_2 [15], isobutane [24], Ar [24], and He [24] are also displayed. The temperature dependence of ${}_1Z^{\mathrm{PO}}_{\mathrm{eff}}$ obviously differs from that of Λ_2 for many other gases and from that obtained with SAG. It is conceivable that p-wave scattering is not negligible in the second path for Ps–Xe collisions.

V. CONCLUSION

We find that the annihilation rate via ortho-para Ps spin conversion due to spin-orbit interaction during Ps–Xe collisions strongly depends on the temperature as being proportional to $T^{2.1}$. Assuming that spin conversion occurs only for p-wave scattering and that Ps atoms are thermalized to a Maxwell-Boltzmann velocity distribution, the experimental results agree well with the theoretical estimate. In our method, the components of the partial wave expansion can be compared with the annihilation rates via the paths by utilizing the Zeeman mixing. This system would bring further cooperative progresses in both experiments and theories. In addition, we find that the pick-off annihilation rate during Ps–Xe collision increases by 130 ± 30% with an increase in temperature from 300 to 623 K. This increase is a dependence much stronger than that observed in other gases.

ACKNOWLEDGMENT

We gratefully acknowledge financial support from the Japan Society for the Promotion of Science (KAKENHI, 23654114).

[1] R. S. Vallery, P. W. Zitzewitz, and D. W. Gidley, Phys. Rev. Lett. **90**, 203402 (2003).
[2] Y. Kataoka, S. Asai, and T. Kobayashi, Phys. Lett. B **671**, 219 (2009).
[3] G. S. Adkins, R. N. Fell, and J. Sapirstein, Phys. Rev. Lett. **84**, 5086 (2000).
[4] B. A. Kniehl and A. A. Penin, Phys. Rev. Lett. **85**, 1210 (2000).
[5] A. H. Al-Ramadhan and D. W. Gidley, Phys. Rev. Lett. **72**, 1632 (1994).
[6] A. Czarnecki, K. Melnikov, and A. Yelkhovsky, Phys. Rev. Lett. **83**, 1135 (1999).
[7] T. Hyodo, T. Nakayama, H. Saito, F. Saito, and K. Wada, Phys. Status Solidi C **6**, 2497 (2009).
[8] G. Laricchia and H. R. J. Walters, Riv. Nuovo Cimento Soc. Ital. Fis. **35**, 305 (2012).
[9] J. Mitroy and S. A. Novikov, Phys. Rev. Lett. **90**, 183202 (2003).
[10] M. Charlton, Rep. Prog. Phys. **48**, 737 (1985).
[11] H. Saito and T. Hyodo, Phys. Rev. Lett. **97**, 253402 (2006).
[12] M. Kakimoto, T. Hyodo, and T. B. Chang, J. Phys. B **23**, 589 (1990).
[13] N. Shinohara, N. Suzuki, T. Chang, and T. Hyodo, Phys. Rev. A **64**, 042702 (2001).
[14] M. Kakimoto, T. Hyodo, T. Chiba, T. Akahane, and T. B. Chang, J. Phys. B **20**, L107 (1987).
[15] R. F. Kiefl, in *Positron Annihilation*, edited by P. G. Coleman, S. C. Sharma, and L. M. Diana (North-Holland, Amsterdam, 1982), p. 690.
[16] S. J. Tao, S. Y. Chuang, and J. Wilkenfeld, Phys. Rev. A **6**, 1967 (1972).
[17] S. Y. Chuang and S. J. Tao, Phys. Rev. A **9**, 989 (1974).
[18] K. F. Canter, J. D. McNutt, and L. O. Roellig, Phys. Rev. A **12**, 375 (1975).
[19] R. A. Fox, K. F. Canter, and M. Fishbein, Phys. Rev. A **15**, 1340 (1977).
[20] J. D. McNutt, V. B. Summerour, A. D. Ray, and P. H. Huang, J. Chem. Phys. **62**, 1777 (1975).
[21] T. Kawaratani, Y. Nakayama, and T. Mizogawa, Phys. Rev. A **37**, 2855 (1988).
[22] K. F. Canter and L. O. Roellig, Phys. Rev. A **12**, 386 (1975).
[23] G. Laricchia, M. Charlton, C. D. Beling, and T. C. Griffith, J. Phys. B **20**, 1865 (1987).
[24] R. S. Vallery, A. E. Leanhardt, M. Skalsey, and D. W. Gidley, J. Phys. B **33**, 1047 (2000).
[25] J. D. McNutt, W. W. Kinnison, and A. D. Ray, J. Chem. Phys. **60**, 4730 (1974).
[26] S. C. Sharma, J. D. McNutt, A. Eftekhari, and R. A. Heji, J. Chem. Phys. **75**, 1226 (1981).
[27] G. R. Heyland, in *Positron Scattering in Gases*, edited by M. R. C. McDowell and J. W. H. Humberston, Vol. 18 (Plenum, New York, 1984), p. 99.
[28] E. P. Liang and C. D. Dermer, Opt. Commun. **65**, 419 (1988).
[29] K. Michishio, T. Tachibana, R. H. Suzuki, K. Wada, A. Yanagishita, and T. Hyodo, Appl. Phys. Lett. **100**, 254102 (2012).
[30] H. Saito, T. Nakayama, and T. Hyodo, J. Phys.: Conf. Ser. **194**, 012038 (2009).
[31] Y. Nagashima, M. Kakimoto, T. Hyodo, K. Fujiwara, A. Ichimura, T. Chang, J. Deng, T. Akahane, T. Chiba, K. Suzuki, B. T. A. McKee, and A. T. Stewart, Phys. Rev. A **52**, 258 (1995).
[32] G. Poelz and R. Riethmuller, Nucl. Instrum. Methods **195**, 491 (1982).
[33] H. Saito, Y. Nagashima, T. Kurihara, and T. Hyodo, Nucl. Instrum. Methods A **487**, 612 (2002).
[34] H. Saito and T. Hyodo, Radiat. Phys. Chem. **68**, 431 (2003).
[35] H. Saito and T. Hyodo, Phys. Rev. Lett. **90**, 193401 (2003).
[36] I. A. Ivanov, J. Mitroy, and K. Varga, Phys. Rev. A **65**, 032703 (2002).